

Convective variability in real mid-latitude weather

August 30, 2016

1 Introduction

1.1 Motivation

Physical processes which occur on scales smaller than the grid spacing of a numerical model typically have to be parameterized. One such process is convection, which acts to restore stability in the atmosphere and is also the cause of significant amounts of precipitation. Parameterizations represent the effect of these sub-grid scale processes on the resolved scales is represented. Traditionally, this is done in a deterministic way, where the average, most likely, sub-grid effect given a certain large-scale forcing is described. If the sampling size of the unresolved features is large enough, the fluctuations about this mean are indeed small and negligible. So, for example, a grid box of a climate model with several hundreds of kilometers in size contains many convective features, typically 1-10 km in size. Global weather models nowadays, however, have grid spacings on the order of 10 km. Here the sampling size becomes insufficient and the fluctuation about a mean state are significant. Ignoring these fluctuations can lead to systematic biases in the non-linear atmosphere (e.g. Berner et al., 2016) and can also lead to an under-representation of extreme events. Furthermore, in an ensemble system, completely deterministic models are severely underdispersive and, therefore, unreliable.

Stochastic parameterizations aim to solve the problems outlined above. Here, randomness is introduced to represent the variability associated with sub-grid processes. In an ad hoc manner this has been done successfully in medium-range weather prediction for almost two decades (Buizza et al., 1999; Berner et al., 2009). These ad hoc methods, however, are finely tuned to give the appropriate spread-skill relation, and do not actually represent the variability associated with a certain physical process. A more physical way of constructing a stochastic parameterization is to explicitly include a physical model of the uncertainty in the formulation of a parameterization. To get a full representation of the complete model uncertainty this has to be done for every parameterized process individually. Several approaches to get a physical model of the underlying uncertainty of convection have been tried. Dorrestijn et al. (2015) and Gottwald et al. (2016) used conditional Markov chains to describe the transition from one cloud-state to another for several micro-nodes in a GCM grid box. The transition probabilities are dependent on some large scale indicator, in their case the large scale vertical velocity, and the exact values are calculated from observations. This approach allows them to calculate a fraction of deep convective clouds for each grid-box, which can then be used to estimate mass flux for use in a convective parameterization. The advantage of using conditional

Markov chains is that they inherently have memory. Application in a simple GCM shows improvements in the distribution of precipitation, and some improvements for equatorial waves (Dorrestijn et al., 2016).

One attempt do formulate such a physically-based stochastic parameterization for convection is described now.

1.2 The Craig and Cohen (2006) theory and its application in Plant and Craig (2008)

The (Craig and Cohen, 2006, CC06) theory aims to quantify the mass flux fluctuations of a cloud field in convective equilibrium. Convective equilibrium implies that the average properties of the convection are determined by the large-scale forcing. In more detail, the average total mass flux $\langle M \rangle$ is a function of the large-scales. Other assumptions are: (a) the mean mass flux per cloud $\langle m \rangle$ does not depend on the large-scale forcing, only the mean number of clouds $\langle N \rangle$ does; (b) non-interacting clouds: Cloud are spatially separated (no clustering) and do not influence each other. (c) Equal a priori probabilities: This statistical equilibrium assumption implies that “that clouds are equally likely to occur in any location and with any mass flux”. Using these arguments as a basis, a statistical theory is constructed for the distributions of N and m :

$$P(N) = \frac{\langle N \rangle^N}{N!} e^{-\langle N \rangle} \quad (1)$$

$$P(m) = \frac{1}{\langle m \rangle} e^{-m/\langle m \rangle} \quad (2)$$

Combing these, the distribution of the total mass flux M is given by

$$P(M) = \left(\frac{\langle N \rangle}{\langle m \rangle} \right)^{1/2} e^{-\langle N \rangle} M^{-1/2} e^{-M/\langle m \rangle} I_1 \left[2 \left(\frac{\langle N \rangle}{\langle m \rangle} M \right)^{1/2} \right], \quad (3)$$

where $I_1(x)$ is the modified Bessel function of order 1. For large (small) values of $\langle N \rangle$ the shape of this function resembles a Gaussian (Poisson) distribution. It is also possible to derive an equation for the normalized variance of M :

$$\mu_2 = \frac{\langle (\delta M)^2 \rangle}{\langle M \rangle^2} = \frac{2}{\langle N \rangle} \quad (4)$$

Always note that $\langle M \rangle = \langle N \rangle \langle m \rangle$. Eq. 4 can be derived directly from Eq. 3 or from the theory of random sums (Taylor and Karlin, 1998, p.70ff): Assume $X = \xi_1 + \dots + \xi_N$ where ξ_k and N have the finite moments $E[\xi_k] = \mu$, $Var[\xi_k] = \sigma^2$ and $E[N] = \nu$, $Var[N] = \tau^2$. Then the first and second moment of X are $E[X] = \mu\nu$, $Var[X] = \nu\sigma^2 + \mu^2\tau^2$.

The theoretical predictions above were tested against numerical simulations in radiative-convective equilibrium (RCE) by Cohen and Craig (2006). The results of these simulations agreed very well with the theory. The error in μ_2 is around 10%, with $\mu_2 \langle N \rangle \approx 1.6$. Other studies introduced time-varying forcings and looked at the differences in mass flux statistics as described below.

In the (Plant and Craig, 2008, PC08) stochastic parameterization approach, the exponential m distribution (Eq. 2) is used to create a random population of plumes for

each grid-box consistent with a large scale $\langle M \rangle$. From this distribution the large-scale tendencies are then computed as the sum of the cloud model output for each plume. $\langle m \rangle = 2 \times 10^7 \text{ kg s}^{-1}$ is assumed to be a constant. This assumption is motivated by RCE simulations (e.g. Cohen and Craig, 2006). The theoretical prediction for the variance of M (Eq. 4) is not explicitly used in PC08, but comes from the exponential m distribution combined with the random initiation of new clouds. The cloud life time is set to 45 minutes for all clouds.

The PC08 scheme has been tested in a GCM study with some success, improving the precipitation patterns and equatorial waves (Wang et al., 2016).

1.3 Deviations from theory in other studies

Two studies looked at the deviations from the CC06 predictions in their simulations of convection with a time varying forcing: Davies (2008) and Davoudi et al. (2010).

1.3.1 Davies (2008)

She used a model with 1km resolution, a prescribed radiative cooling and time-varying surface fluxes or temperature. For the reference RCE simulation she found $\mu_2 \langle N \rangle \approx 1.5$ at 3 km, a deviation of 10% in μ_2 , which is in agreement with CC06. When looking at their time-varying simulations, they see that μ_2 is increased (about 2.2) 1h after convection is first triggered and at around 15UTC. They find that at the triggering time and at 18UTC there is strong clustering at scales from 5–20 km.. At the time of maximum convection (12UTC), the RDF is almost uniform and $\mu_2 \approx 0.7$. She argues that the deviation from the predicted variance can be largely explained by clustering.

1.3.2 Davoudi et al. (2010)

They used a similar model setup to CC06, but with a diurnal cycle through interactive radiation, but with a fixed SST. In their Fig. 13, they show their values of $\mu_2 \langle N \rangle$ for different heights. They find that for $z < 8$ km, this value is less than two. Additionally, in their Fig. 12. they plot histograms of $P(M)$ from their data. They then fit Eq. 3 with $\langle M \rangle$ and $\langle N \rangle$ as free parameters. When they compare these fitted values to the calculated values of $\langle M \rangle$ and $\langle N \rangle$ from their data, they find that $\langle M \rangle$ is similar but the fitted $\langle N \rangle$ is larger than the observed $\langle N \rangle$. They state that “Therefore, predictions of μ_2 are smaller than the corresponding normalized variance from the data. Figure 13 demonstrates that the variance, as well as skewness, is underestimated by the theory close to the cloud base and for the range of altitudes in $z \in [2, 8]$ km.”

They then look at two clustering metrics. First, the radial distribution function (their Fig. 14), where they find strong clustering for 5-10 km. Second, $\alpha = \frac{\sigma_N^2}{\langle N \rangle}$, where they find values of about 110% at cloud base, which is in agreement with the findings by CC06 and Davies (2008).

1.4 Research questions

The simple theory of CC06 has been shown to predict the convective variability well in highly idealized simulations and has been used as the basis for the PC08 stochastic con-

vection scheme with some success. Other studies have looked at the influence of a time varying forcing and clustering on convective variability, but these studies also used highly idealized setups. So far, there has been no estimate of the convective variability of a “real” weather situation. Particularly the mid-latitudes deviate from RCE simulations in many important ways. The goal of this study is to quantitatively investigate the convective variability in “real” mid-latitude weather and compare the results to the theoretical predictions of CC06. More specifically, the research question is:

RQ1 How does the convective variability of “real” mid-latitude weather situations compare to the predictions of CC06?

Hypothesis There will be some deviations from the theoretical predictions similar to what Cohen and Craig (2006), Davies (2008) and Davoudi et al. (2010) found.

If this hypothesis is true, a follow up research questions is:

RQ1.1 To what extent can the deviations from the predicted variability be quantitatively explained by clustering?

Hypothesis Clustering can explain most of the deviations from the predicted variance.

If this latest hypothesis is not true, then the next follow up research question is:

RQ1.2 Can other parameters be found to explain the remaining deviations from theory?

Hypothesis External parameters like the convective timescale of orography can explain some of the deviations.

The hope is that by finding these factors in the second hypothesis, stochastic parameterizations can be constructed which include a better representation of the real variability of convection.

2 Methods

2.1 General research strategy

We will use convection-permitting simulations of real weather situations over Germany. A stochastic boundary-layer scheme will be used to create an ensemble where the convection is displaced. We will then use these ensembles to calculate statistics similar to those in CC06 and compare the results to the theoretical prediction. To explain deviations from the theory, we will try to find meaningful measures to characterize the synoptic situation of the case studies and to correlate them with the deviations.

2.2 Numerical experiments

The model used is the COSMO model with 2.8 km horizontal grid spacing Δx and operational COSMO-DE settings with one exception, the stochastic boundary-layer scheme which will be described below. The domain size is 357 grid points in either direction with the domain centered at 10E and 50N. For the analysis a 256 by 256 grid point domain (roughly 717km) at the center of the simulation domain is considered. The 50 grid point gap to the boundary ensures that boundary effects are minimal.

Initial and boundary conditions are taken from the operational COSMO-EU (7km) deterministic forecast with a boundary condition update frequency of 1 h. All runs are started at 00UTC and are run for 24 h. A 20 member ensemble is created by setting a

different random number seed in the stochastic boundary-layer scheme for each member. Otherwise, all members are identical, making sure that the large-scale condition are the same and only the convection is shuffled around.

2.2.1 The PSPturb turbulence scheme

The physically-based stochastic perturbation boundary-layer scheme (PSPturb) is described and tested in (Kober et al., 2016, KC16). A brief outline is given here now.

The PSPbl scheme is additive:

$$\left(\frac{\partial \Phi}{\partial t} \right)_{\text{total}} = \left(\frac{\partial \Phi}{\partial t} \right)_{\text{parameterized}} + \eta \sigma_{\left(\frac{\partial \Phi}{\partial t} \right)_{\text{parameterized}}} \quad (5)$$

These perturbations are process-specific, so for each parameterized process the perturbations have to be calculated separately. The last term in the equation above contains a random number $\eta = N(0, 1)$ and the standard deviation of the parameterized tendencies. The random number field has a horizontal correlation length of $5\Delta x$, the effective resolution and is held constant for 10 minutes and then drawn again from scratch. This represents a typical eddy turnover time in the boundary layer. In KC16 the standard deviation term is approximated by

$$\sigma_{\left(\frac{\partial \Phi}{\partial t} \right)_{\text{parameterized}}} = \alpha_{\text{const}, \Phi} \frac{l_\infty}{5\Delta x} \frac{1}{dt} \sigma_\Phi, \quad (6)$$

where $l_\infty = 150$ m is the mixing length describing the average size of an eddy. The term σ_Φ is the sub-grid scale standard deviation. For the turbulence perturbations the considered variables are vertical velocity w , potential temperature θ and humidity q . The standard deviations are calculated in the turbulence parameterization (see KC06 for details). The factor $\frac{l_\infty}{5\Delta x} \propto \frac{1}{\sqrt{N_{\text{eddy}}}}$ scales the variability according to number of unresolved eddies similar to Eq. 4. The factor $\frac{1}{dt}$ converts the term into a tendency term dependent on the time step. Finally, a scaling factor $\alpha_{\text{const}, \Phi}$ is included for tuning purposes and should be of order one.

2.3 Case studies

The case studies are all from a recent, convectively active period over Central Europe in May/June 2016 with one exception: We also considered 1 July 2009, which is the test case used in Kober et al. (2016), since this day is a good example of weakly forced diurnal convection.

2.4 Analyses

2.4.1 Heigh level of analyses

Since the height above sea level is not constant for our simulations, the questions arises which level to take for domain averages. Height above sea level would not be a good choice since the vertical location of the statistics since the boundary layer depends on the height above ground level, which would also not be a good choice since the tropopause level is

largely unaffected by the height above ground level. A logical choice is to use model levels. In the COSMO model the model levels are terrain-following. In the lower troposphere, they are largely parallel to the ground, but at around 10 km, they are largely parallel to sea level. To pick certain levels, we look at a column above the ocean and search for the closes model level to a height above sea level.

2.4.2 Identification of clouds and calculation of cloud statistics

To identify clouds, first the fields are converted to binary fields by applying a threshold. Two different fields and thresholds are used for this study: (1) Vertical velocity $w > 1 \text{ m s}^{-1}$ plus a positive cloud water content $q_c > 0 \text{ kg kg}^{-1}$. The height chosen is 2500 m, which is above the level of shallow convection. The criterion is denoted by the letter m (for mass flux). This criterion was also used by Cohen and Craig (2006) and Davoudi et al. (2010). (2) Instantaneous precipitation rate $pr > 0.001 \text{ mm h}^{-1}$. This is a surface variable. This criterion is denoted by the letter p . As of now, only criterion (1) is used!

Contiguous areas are then identified as clouds using a 4-point segmentation algorithm. Optionally, “overlapping” clouds are identified with the local maximum method, followed by a watershed algorithm to find the extent of each separated cloud. If this step is (not) applied, the label (“nowater”) “water” is used.

For each identified cloud $k = 1, \dots, N_{\text{cld},i}$ in each ensemble member $i = 1, \dots, N_{\text{ens}}$ a cloud size σ_k is determined as

$$\sigma_k = n_{px} \Delta x^2, \quad (7)$$

where N_{px} is the number of pixels for each cloud k . Furthermore, the mass flux per cloud m_k is computed for criterion (1) as

$$m_k = \Delta x^2 \sum_l^{N_{px}} w_l \rho_l, \quad (8)$$

where ρ is density.

2.4.3 Calculation of radial distribution functions

A radial distribution function (RDF) is calculated at each time for each member separately. To do this, the center of mass for each cloud is identified. For these points a two-dimensional pair correlation is computed, where the step size of the search function is $2\Delta x$ and the maximum search radius is $30\Delta x$. The output is normalized, so that a completely randomly distributed field would give an RDF of 1 at all radii. The results are averaged over the ensemble members to give one RDF at each time.

2.4.4 Calculation of ensemble means and variances

For the variance calculations, a coarse-graining is applied to create coarse boxes $j = 1, \dots, N_{\text{box},n}$ edge lengths of $n = 256, 128, 64, 32, 16, 8$ and $4\Delta x$, where $N_{\text{box},n} = n^2$. No neighborhoods smaller are considered, since these would be significantly below the effective resolution of the model (Bierdel et al., 2012). Ensemble statistics are then calculated for each box j . The sample variance is computed with

$$\langle (\delta M)^2 \rangle_{j,n} = \frac{1}{N_{\text{ens}} - 1} \sum_{i=1}^{N_{\text{ens}}} (M_{i,j,n} - \langle M \rangle_{j,n})^2, \quad (9)$$

where the ensemble mean is

$$\langle M \rangle_{j,n} = \frac{1}{N_{\text{ens}}} \sum_{i=1}^{N_{\text{ens}}} M_{i,j,n}. \quad (10)$$

These calculations are done analogously for N . The total mass flux per box per member $M_{i,j,n}$ is given by

$$M_{i,j,n} = \sum_{k=1}^{N_{\text{cld},i,j,n}} m_{k,i,j,n}. \quad (11)$$

To deal with clouds at the boundaries of the coarse-fields, the centers of mass for each cloud is first identified. Then the m_k is attributed to that one point in space. Therefore, the coarse box which contains the center of mass also contains the entire cloud, while the other box does not contain any of the cloud. $N_{i,j,n} = N_{\text{cld},i,j,n}$ is simply the number of clouds which fall into each box.

To compute statistics for m a different approach is taken. Here the clouds in all members for each box are considered together to calculate the variance and mean. The total number of clouds over all ensemble members is denoted by $N_{\text{cldtot}} = \sum_{i=1}^{N_{\text{ens}}} N_{\text{cld},i,j,n}$.

$$\langle (\delta m)^2 \rangle_{j,n} = \frac{1}{N_{\text{cldtot}} - 1} \sum_{k=1}^{N_{\text{cldtot}}} (m_{k,j,n} - \langle m \rangle_{j,n})^2, \quad (12)$$

where the mean is

$$\langle m \rangle_{j,n} = \frac{1}{N_{\text{cldtot}}} \sum_{k=1}^{N_{\text{cldtot}}} m_{k,j,n}. \quad (13)$$

2.4.5 Sampling issues

Since we are sampling a distribution with a limited number of data points N_{ens} , sampling issues arise when $\langle N \rangle$ becomes small ($\approx \frac{1}{N_{\text{ens}}}$). In particular, if only one member contains a cloud chances are that the real $\langle N \rangle < \frac{1}{N_{\text{ens}}}$ and we therefore overestimate the mean mass flux $\langle M \rangle$. To avoid this issue, a criterion is introduced where at least 5 out of 20 ensemble members must contain at least one cloud. *This threshold is a quick fix and should be determined statistically.*

2.4.6 Comparison with prediction

To compare the obtained values to the theoretical predictions (**RQ1**), the normalized variance for each coarse box j at each coarsening scale n is calculated as

$$\mu_{2,j,n} = \frac{\langle (\delta M)^2 \rangle_{j,n}}{\langle M \rangle_{j,n}^2}. \quad (14)$$

The normalized variance is then plotted against the RHS of Eq. 4 $\frac{2}{\langle N \rangle_{j,n}}$. The theory from Eq.4 predicts a slope of 2 for the resulting scatter plot. To get a quantitative comparison of the simulation results and theory, the fraction is calculated as

$$\frac{\mu_{2,j,n} \langle N \rangle_{j,n}}{2}. \quad (15)$$

To get a summary measure of how the normalized variance compares to the predicted value for each scale n , the mean $\frac{\mu_2\langle N \rangle}{2}$ is calculated:

$$\overline{\frac{\mu_2\langle N \rangle}{2}}_n = \frac{1}{2N_{\text{box}}n} \sum_{j=1}^{N_{\text{box}}n} \mu_{2,j,n} \langle N \rangle_{j,n}. \quad (16)$$

According to theory this value should be 1. Similarly the standard deviation is calculated as

$$\text{std}\left(\frac{\mu_2\langle N \rangle}{2}\right)_n = \sqrt{\frac{1}{N_{\text{box}}n - 1} \sum_{j=1}^{N_{\text{box}}n} \left(\frac{\mu_{2,j,n}\langle N \rangle_{j,n}}{2} - \overline{\frac{\mu_2\langle N \rangle}{2}}_n \right)^2}. \quad (17)$$

Following Davoudi et al. (2010), we calculate $\alpha_{j,n} = \frac{\langle (\delta N)^2 \rangle_{j,n}}{\langle N \rangle_{j,n}}$ as a measure of the clustering, or deviation from a Poisson distribution:

$$\bar{\alpha}_n = \frac{1}{N_{\text{box}}n} \sum_{j=1}^{N_{\text{box}}n} \frac{\langle (\delta N)^2 \rangle_{j,n}}{\langle N \rangle_{j,n}}. \quad (18)$$

To include the effects of $\alpha \neq 1$ for μ_2 , we derive an adjusted equation from the theory of random sums (see above), which states:

$$\langle (\delta M)^2 \rangle = \langle N \rangle \langle (\delta m)^2 \rangle + \langle m \rangle^2 \langle (\delta N)^2 \rangle \quad (19)$$

Here we assume an exponential distribution for m , so that $\langle (\delta m)^2 \rangle = \langle m \rangle^2$. To test this assumption the ratio

$$\frac{1}{N_{\text{box}}n} \sum_{j=1}^{N_{\text{box}}n} \frac{\langle (\delta m)^2 \rangle_{j,n}}{\langle m \rangle_{j,n}^2} \quad (20)$$

is calculated for every n . We do not assume a Poisson distribution for N , which would give $\langle (\delta N)^2 \rangle = \langle N \rangle$ and lead to Eq. 4. Together with $\langle M \rangle = \langle m \rangle \langle N \rangle$ we can write:

$$\langle (\delta M)^2 \rangle = \frac{\langle M \rangle^2}{\langle N \rangle^2} (\langle N \rangle + \langle (\delta N)^2 \rangle) \quad (21)$$

And therefore,

$$\tilde{\mu}_2 = \frac{\langle (\delta M)^2 \rangle}{\langle M \rangle^2} = \frac{(\langle N \rangle + \langle (\delta N)^2 \rangle)}{\langle N \rangle^2} = \frac{1 + \alpha}{\langle N \rangle} \quad (22)$$

If N follows a Poisson distribution, this equation is equivalent to Eq. 4. For increased clustering $\alpha > 1$, so therefore $\tilde{\mu}_2 > \mu_2$. With this adjusted equation for the normalized mass flux variance, the clustering which has an effect on N is accounted for. If the clustering explains all of the deviations of μ_2 from theory, then

$$\overline{\frac{\tilde{\mu}_2\langle N \rangle}{1 + \alpha}}_n = \frac{1}{N_{\text{box}}n} \sum_{j=1}^{N_{\text{box}}n} \frac{\mu_{2,j,n}\langle N \rangle_{j,n}}{1 + \alpha_{j,n}} \quad (23)$$

should be 1, which can be tested directly from the data to answer **RQ1.1**.

2.4.7 Calculation of the convective adjustment timescale

The convective timescale was calculated according to Flack et al. (2016). To produce ensemble mean plots of τ_c the fields are calculated for each ensemble member individually and then averaged. This leads to some not-smooth regions at the edges. Furthermore, a minimum precipitation threshold of 0.2 mm h^{-1} is used, which leads to the timescale not being calculated for regions only a few small cells. Therefore, not every variance value can be matched with a timescale value.

2.5 Composites

Composites were computed by averaging over the days in the simulation period.

3 Results

3.1 Weather situation 28 May - 8 June 2016

28 May The synoptic forcing is weak. Over Southern Germany, high values of CAPE build up (around 1000 J/kg). Scattered diurnal convection develops.

29 May At night, some rain is advected from the South. Generally, the wind come from the South. During day, CAPE is high in Eastern Germany. There are both scattered convective cells and more stratiform regions.

30 May - 5 June A low pressure system is stationed over Southern Germany causing easterly advection over Northern Germany. This is coupled with diurnal convection.

6 – 8 June The synoptic forcing is weaker with scattered convective cells.

3.2 Comparison with prediction

The correspondence of the computed variance and the theoretical predictions can be seen in 4.1 and 4.2 (both agree well). (top left) shows mu_2 plotted against $2/N$. The gray line indicates perfect agreement between simulations and predictions. (top right) shows the fraction value of the predicted value. For all n , the mean simulated variance is below the predicted variance. for large and small n the relative variances are lower with an error of around 30%. For n around 100 km, the simulations match the predictions well, with a deviation of 5–10%. The standard deviations of the relative variances increase with n , which is most likely due to the smaller sample size for larger n . These plots allow us to answer **RQ1**. The variances from the numerical simulations deviate from the predictions. In particular the simulated variances are, on average, lower, which is in agreement with previous studies.

In the next step, we look at the correlation between the relative variance and the clustering parameter α (bottom left). There is a clear correlation, indicating that for larger α , so increased clustering, the relative variance is higher. Using this information to calculate an adjusted relative variance (bottom right) gives us the chance to quantify

this effect. The mean relative variances for small and large n are relatively unchanged, but they are lower for n around 100 km. The standard deviations are greatly reduced, particularly for larger n . With regards to **RQ1.1**, these results suggest that clustering, as measured by α , can explain some of the deviations from the theoretical predictions, but not all of them. The theory seems to systematically predict larger variances.

3.3 The diurnal cycle

Next we want to see whether there are significant diurnal cycle correlations in the variances. 4.2 shows the composite evolution of the mean values for the relative variance (top left). There is a diurnal cycle visible with a minimum variance during the day and increased variances in the evening. The diurnal variations are larger for larger n . This corresponds well with the diurnal variation of α (bottom right). The adjusted relative variance (top right) is much smoother, indicating that the clustering accounts for much of the diurnal variability of the relative variance.

References

- Berner, J., G. J. Shutts, M. Leutbecher, and T. N. Palmer, 2009: A Spectral Stochastic Kinetic Energy Backscatter Scheme and Its Impact on Flow-Dependent Predictability in the ECMWF Ensemble Prediction System. *Journal of the Atmospheric Sciences*, **66** (3), 603–626, doi: 10.1175/2008JAS2677.1.
- Berner, J., et al., 2016: Stochastic Parameterization: Towards a new view of Weather and Climate Models. *Bull. Am. Meteorol. Soc.*, URL: <http://dx.doi.org/10.1175/BAMS-D-15-00268.1>.
- Bierdel, L., P. Friederichs, and S. Bentzien, 2012: Spatial kinetic energy spectra in the convection-permitting limited-area NWP model COSMO-DE. *Meteorologische Zeitschrift*, **21** (3), 245–258, doi:10.1127/0941-2948/2012/0319, URL: <http://www.ingentaconnect.com.emedien.ub.uni-muenchen.de/search/article?option1=tka&value1>
- Buizza, R., M. Milleer, and T. N. Palmer, 1999: Stochastic representation of model uncertainties in the ECMWF ensemble prediction system. *Quarterly Journal of the Royal Meteorological Society*, **125** (560), 2887–2908, doi:10.1002/qj.49712556006, URL: <http://doi.wiley.com/10.1002/qj.49712556006>.
- Cohen, B. G. and G. C. Craig, 2006: Fluctuations in an Equilibrium Convective Ensemble. Part II: Numerical Experiments. *Journal of the Atmospheric Sciences*, **63** (8), 2005–2015, doi: 10.1175/JAS3710.1, URL: <http://journals.ametsoc.org/doi/abs/10.1175/JAS3710.1>.
- Craig, G. C. and B. G. Cohen, 2006: Fluctuations in an Equilibrium Convective Ensemble. Part I: Theoretical Formulation. *Journal of the Atmospheric Sciences*, **63** (8), 1996–2004, doi: 10.1175/JAS3709.1, URL: <http://journals.ametsoc.org/doi/abs/10.1175/JAS3709.1>.
- Davies, L., 2008: Self-organisation of convection as a mechanism for memory. Ph.D. thesis.
- Davoudi, J., N. A. McFarlane, and T. Birner, 2010: Fluctuation of Mass Flux in a Cloud-Resolving Simulation with Interactive Radiation. *Journal of the Atmospheric Sciences*, **67** (2), 400–418, doi:10.1175/2009JAS3215.1, URL: <http://journals.ametsoc.org/doi/abs/10.1175/2009JAS3215.1>.
- Dorrestijn, J., et al., 2015: Stochastic Parameterization of Convective Area Fractions with a Multicloud Model Inferred from Observational Data. *Journal of the Atmospheric Sciences*, **72** (2), 854–869, doi:10.1175/JAS-D-14-0110.1, URL: <http://journals.ametsoc.org/doi/10.1175/JAS-D-14-0110.1>.
- Dorrestijn, J., et al., 2016: Stochastic Convection Parameterization with Markov Chains in an Intermediate-Complexity GCM. *Journal of the Atmospheric Sciences*, **73** (3), 1367–1382, doi:10.1175/JAS-D-15-0244.1, URL: <http://journals.ametsoc.org/doi/10.1175/JAS-D-15-0244.1>.
- Flack, D. L. A., R. S. Plant, S. L. Gray, H. W. Lean, C. Keil, and G. C. Craig, 2016: Characterisation of Convective Regimes over the British Isles. *Quarterly Journal of the Royal Meteorological Society*, n/a–n/a, doi:10.1002/qj.2758, URL: <http://doi.wiley.com/10.1002/qj.2758>.
- Gottwald, G. A., K. Peters, and L. Davies, 2016: A data-driven method for the stochastic parametrisation of subgrid-scale tropical convective area fraction. *Quarterly Journal of the Royal Meteorological Society*, **142** (694), 349–359, doi:10.1002/qj.2655, URL: <http://doi.wiley.com/10.1002/qj.2655>.

- Kober, K., G. C. Craig, K. Kober, and G. C. Craig, 2016: Physically Based Stochastic Perturbations (PSP) in the Boundary Layer to Represent Uncertainty in Convective Initiation. *Journal of the Atmospheric Sciences*, **73** (7), 2893–2911, doi:10.1175/JAS-D-15-0144.1, URL: <http://journals.ametsoc.org/doi/10.1175/JAS-D-15-0144.1>.
- Plant, R. S. and G. C. Craig, 2008: A Stochastic Parameterization for Deep Convection Based on Equilibrium Statistics. *Journal of the Atmospheric Sciences*, **65** (1), 87–105, doi:10.1175/2007JAS2263.1, URL: <http://journals.ametsoc.org/doi/abs/10.1175/2007JAS2263.1>.
- Taylor, H. and S. Karlin, 1998: *An introduction to stochastic modeling*. URL: <https://books.google.de/books?hl=en&lr=&id=ppHiBQAAQBAJ&oi=fnd&pg=PP1&dq=An+Introduction+to+Stochastic+Modeling>
- Wang, Y., G. J. Zhang, and G. C. Craig, 2016: Stochastic convective parameterization improving the simulation of tropical precipitation variability in the NCAR CAM5. *Geophysical Research Letters*, **43** (12), 6612–6619, doi:10.1002/2016GL069818, URL: <http://doi.wiley.com/10.1002/2016GL069818>.

4 Figures

All plots for level 30 (about 3000m above ground, unless noted otherwise)

4.1 Example case: June 4

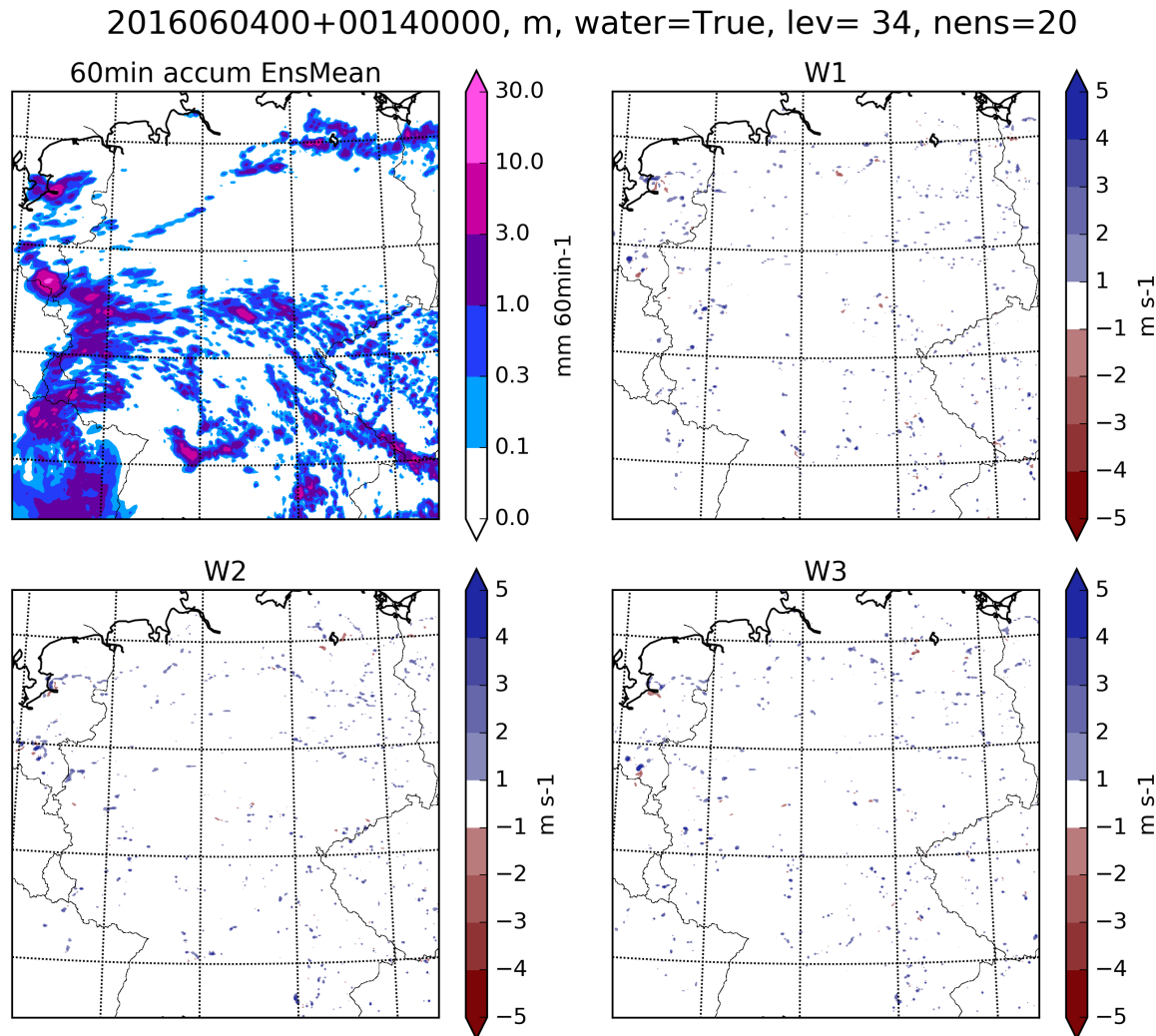


Figure 1: (Top left) Ensemble mean precipitation, (remaining plots) vertical velocity field for the first three ensemble members

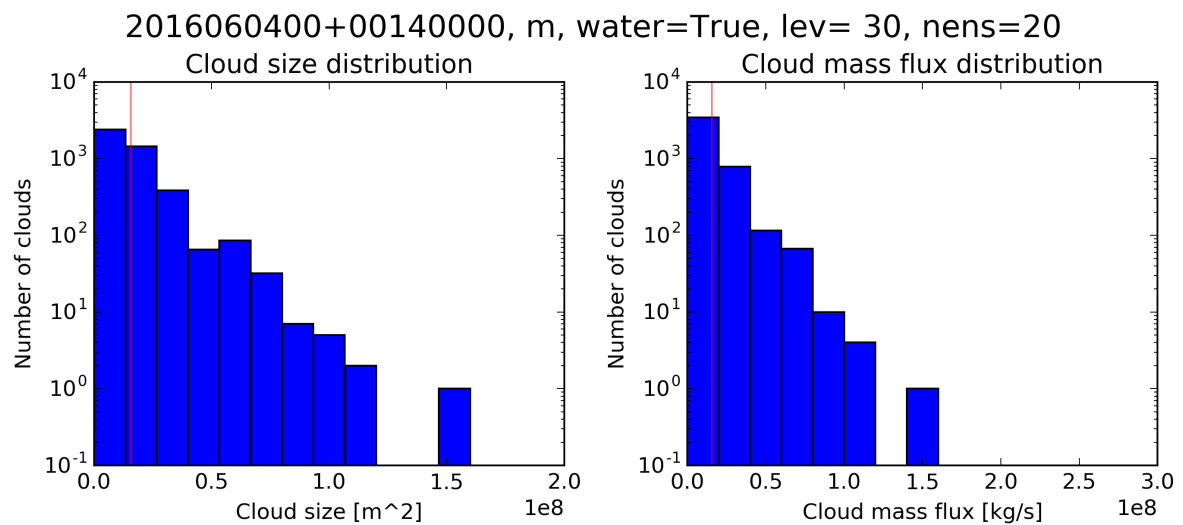


Figure 2: Cloud statistics for one time step (14UTC): (left) Histogram of cloud size (15 bins with width $0.13\text{e}8 \text{ m}^2$) (right) histogram of m (15 bins with width $0.5\text{e}8 \text{ kg/s}$). Red lines show the mean value.

2016060400, m,
water=True, lev= 30, nens=20

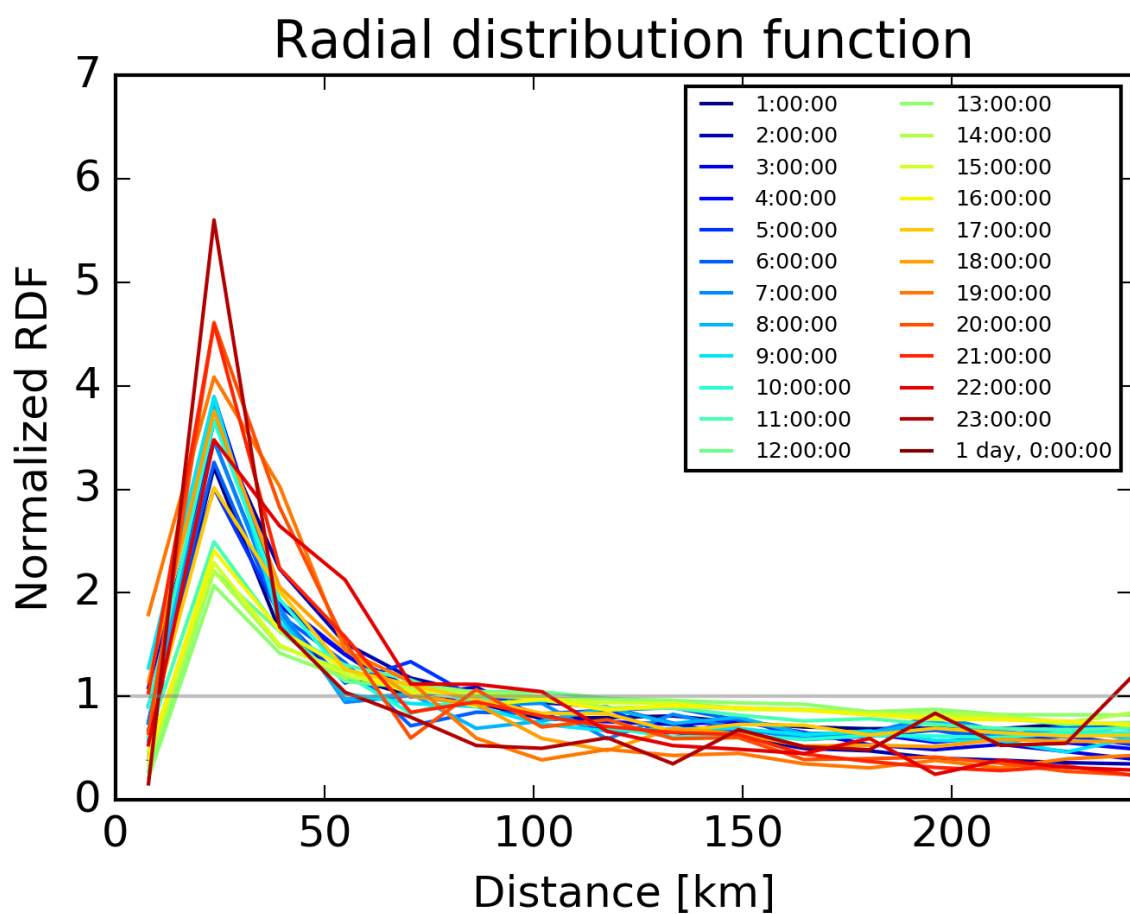


Figure 3: Radial distribution function for each analysis time step

2016060400+00140000, m, water=True, lev= 34, nens=20, n=64

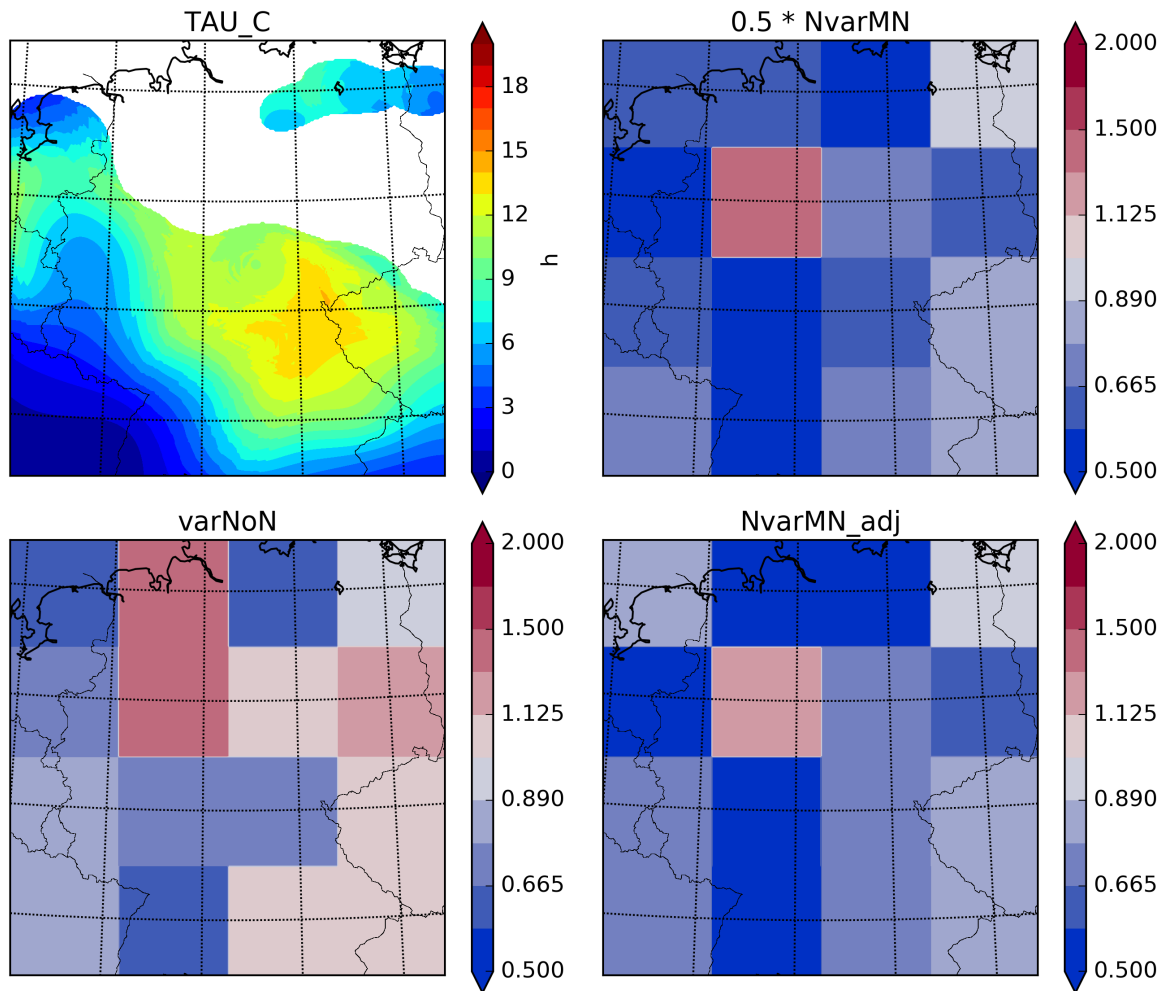


Figure 4: For one time (14UTC) and one $n = 64$: (Top left) Ensemble mean convective timescale, (top right) $\mu_{2,j,n} \langle N \rangle_{j,n}$, (bottom left) $\frac{\langle (\delta N)^2 \rangle_{j,n}}{\langle N \rangle_{j,n}}$ and (bottom right) $\frac{\mu_{2,j,n} \langle N \rangle_{j,n}}{1 + \alpha_{j,n}}$

2016060400, m, water=True, lev= 30, nens=20

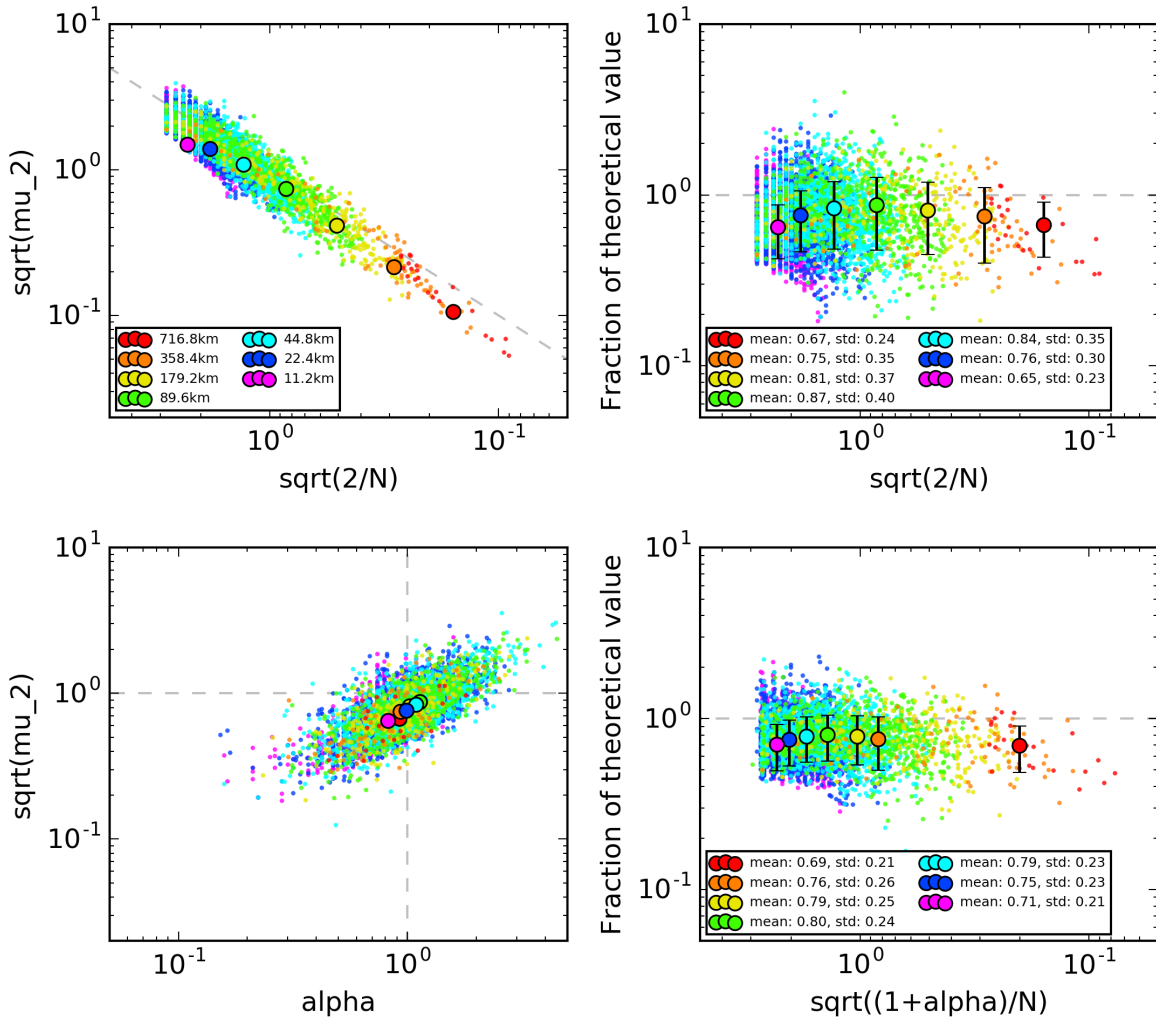


Figure 5: Variance scatter plots: (left) the square root of the normalized variance is plotted against the square root of $1/N$. The gray line represents the theoretical prediction. (right) Percentage fraction of theoretical prediction. Crosses represent the mean value for each scale. The mean is calculated in the log-space.

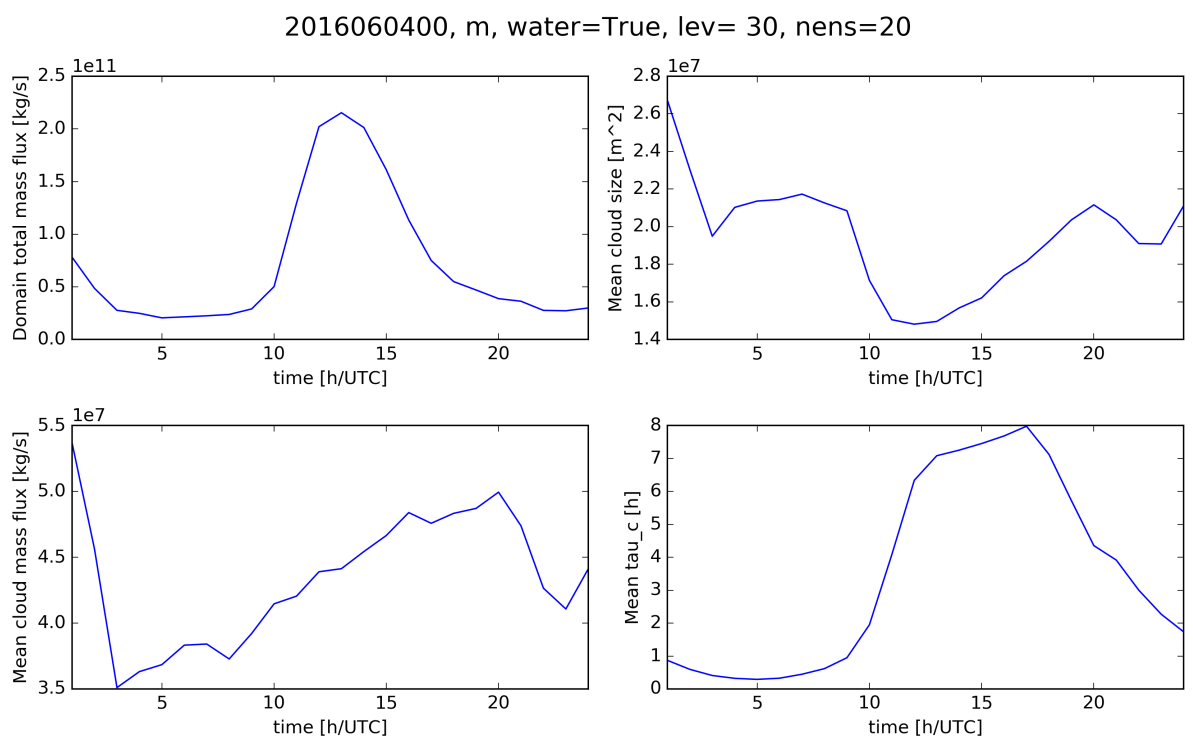


Figure 6: Time evolution of (top left) the total mass flux integrated over the analysis domain, (top right) the mean cloud size, (bottom left) the mean mass flux per cloud (m) and (bottom right) the domain mean convective time scale

2016060400
m, water=True, lev= 30, nens=20

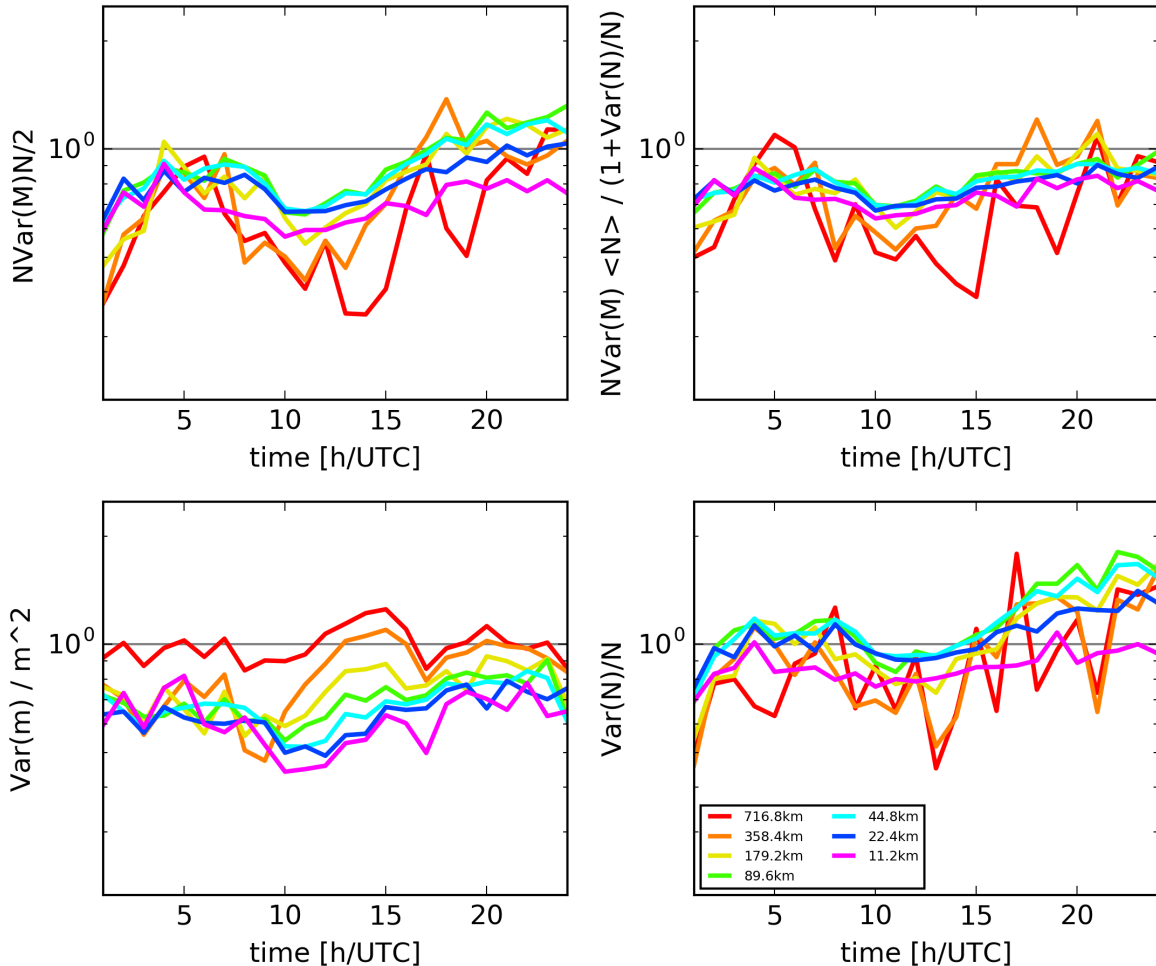


Figure 7: Time evolution of (top left) $0.5 \times \overline{\mu_2(N)}_n$ (see Eq. 16), (top right) $\overline{\frac{\tilde{\mu}_2(N)}{1+\alpha}}_n$ (see Eq. 23), (bottom left) $\frac{1}{N_{\text{box},n}} \sum_{j=1}^{N_{\text{box},n}} \frac{\langle (\delta m)^2 \rangle_{j,n}}{\langle m \rangle_{j,n}^2}$ (see Eq. 20) and (bottom right) $\bar{\alpha}_n$ (see Eq. 18)

4.2 Composite over 12 days

l00_201606100_201606200_201606300_201606400_201
m, water=True, lev= 30, nens=20

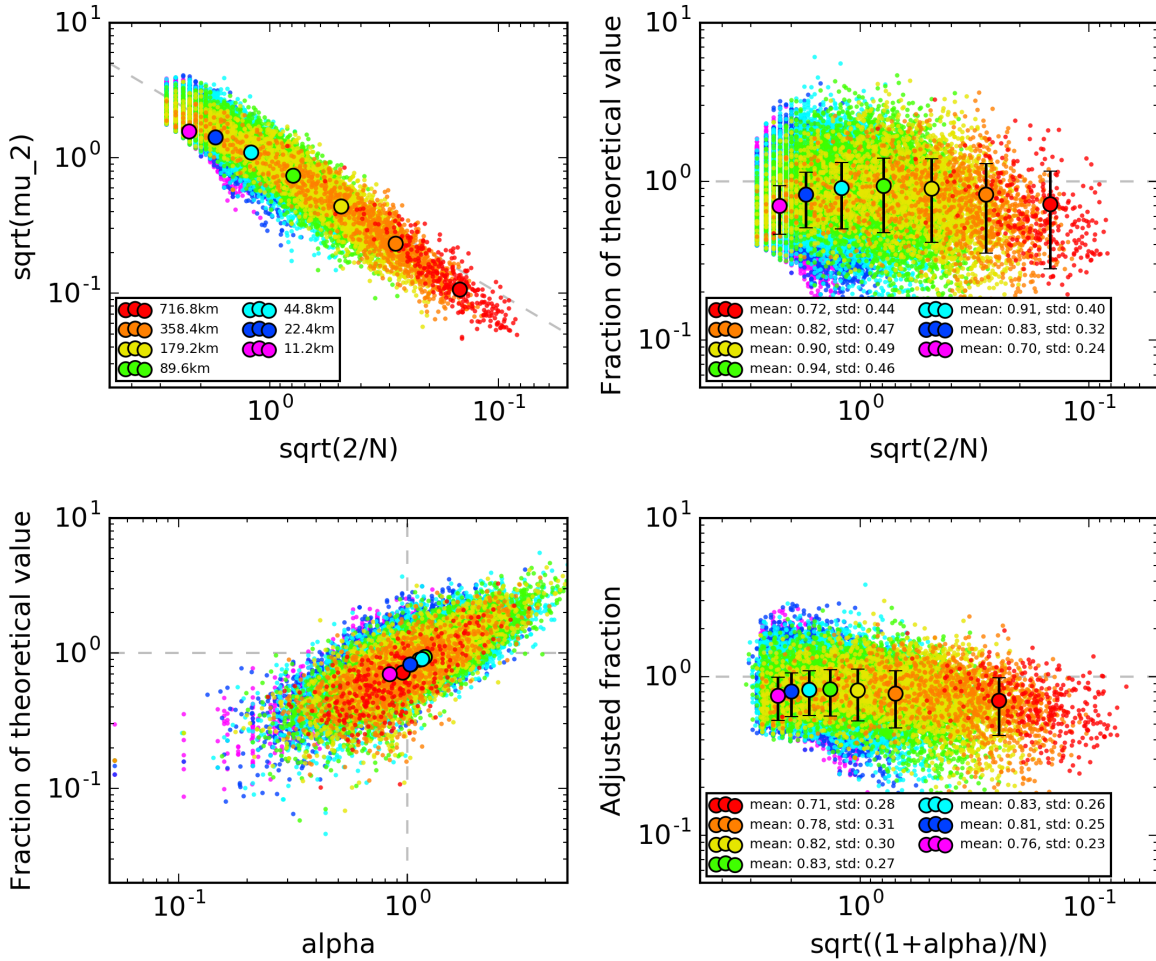


Figure 8: Variance scatter plots: (left) the square root of the normalized variance is plotted against the square root of $1/N$. The gray line represents the theoretical prediction. (right) Percentage fraction of theoretical prediction. Crosses represent the mean value for each scale. The mean is calculated in the log-space.

100_2016060200_2016060300_201606
water=True, lev= 30, nens=20

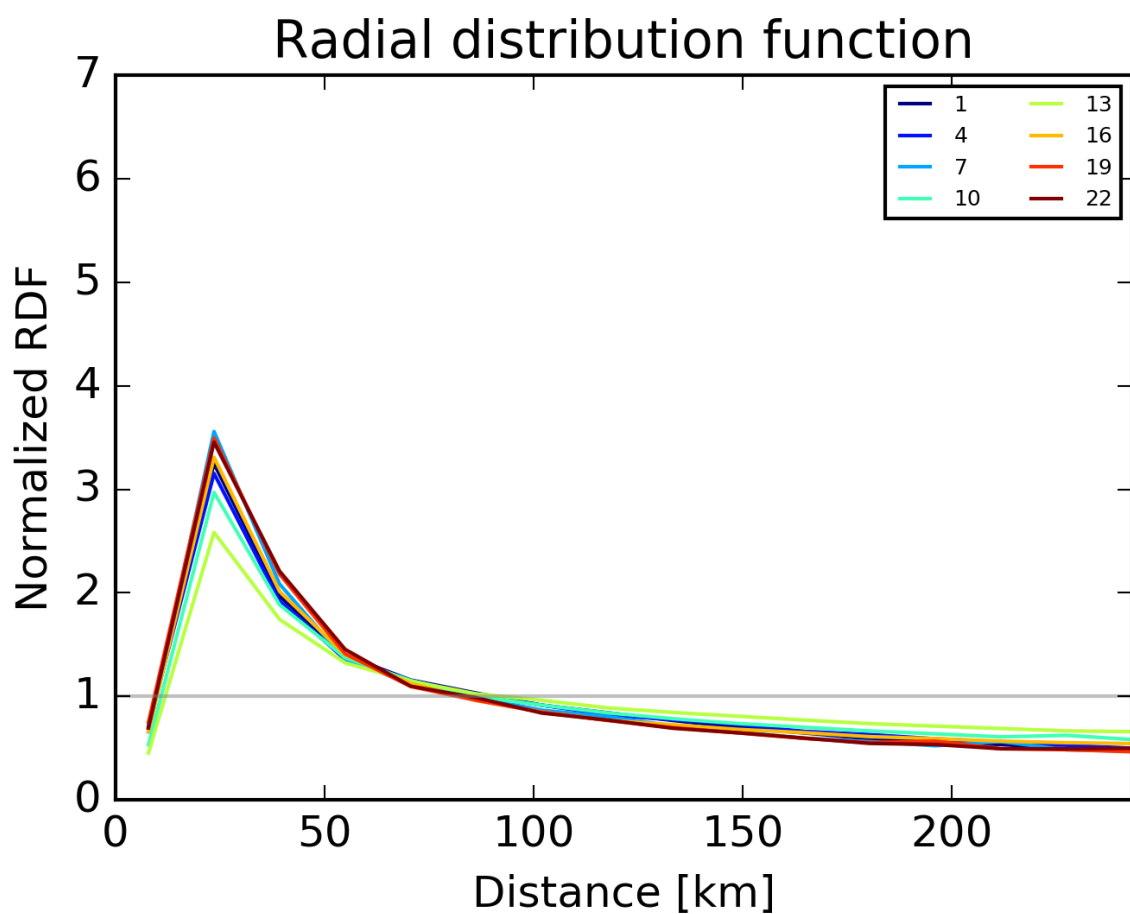


Figure 9: Radial distribution function for each analysis time step

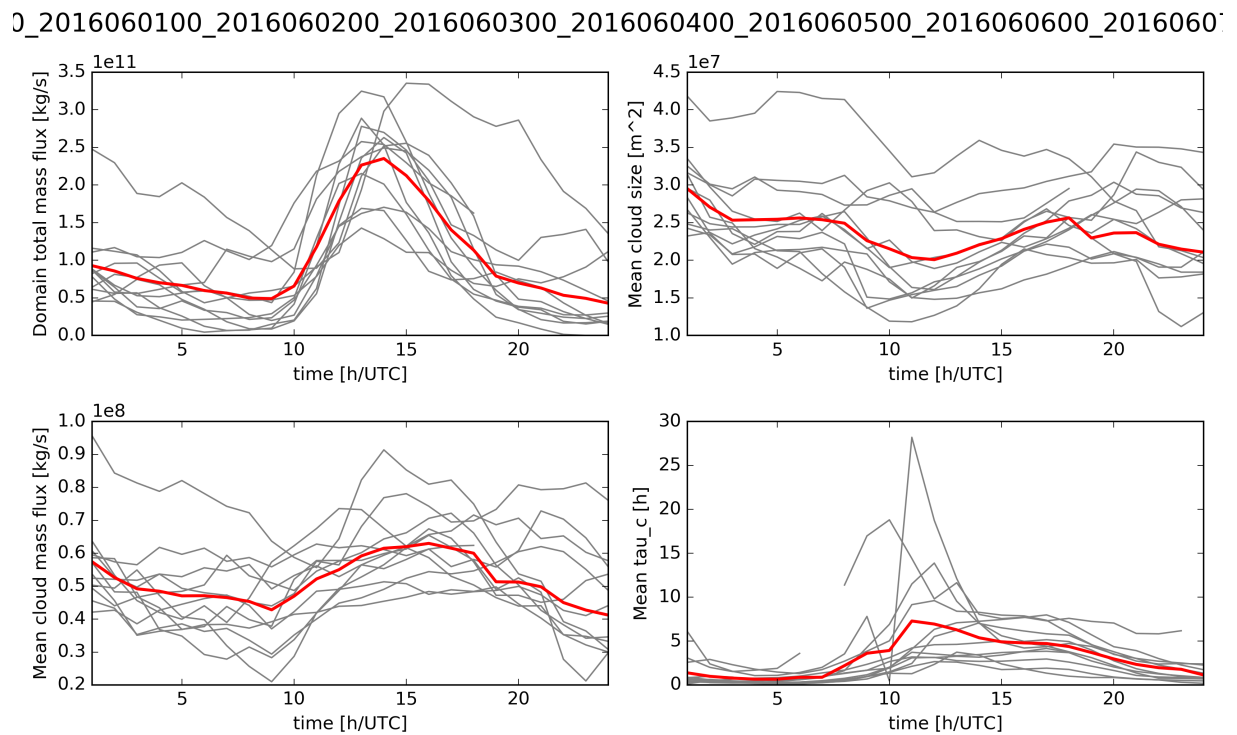


Figure 10: Time evolution of (top left) the total mass flux integrated over the analysis domain, (top right) the mean cloud size, (bottom left) the mean mass flux per cloud $\langle m \rangle$ and (bottom right) the domain mean convective time scale

L00_201606100_201606200_201606300_201606400_201
 m, water=True, lev= 30, nens=20

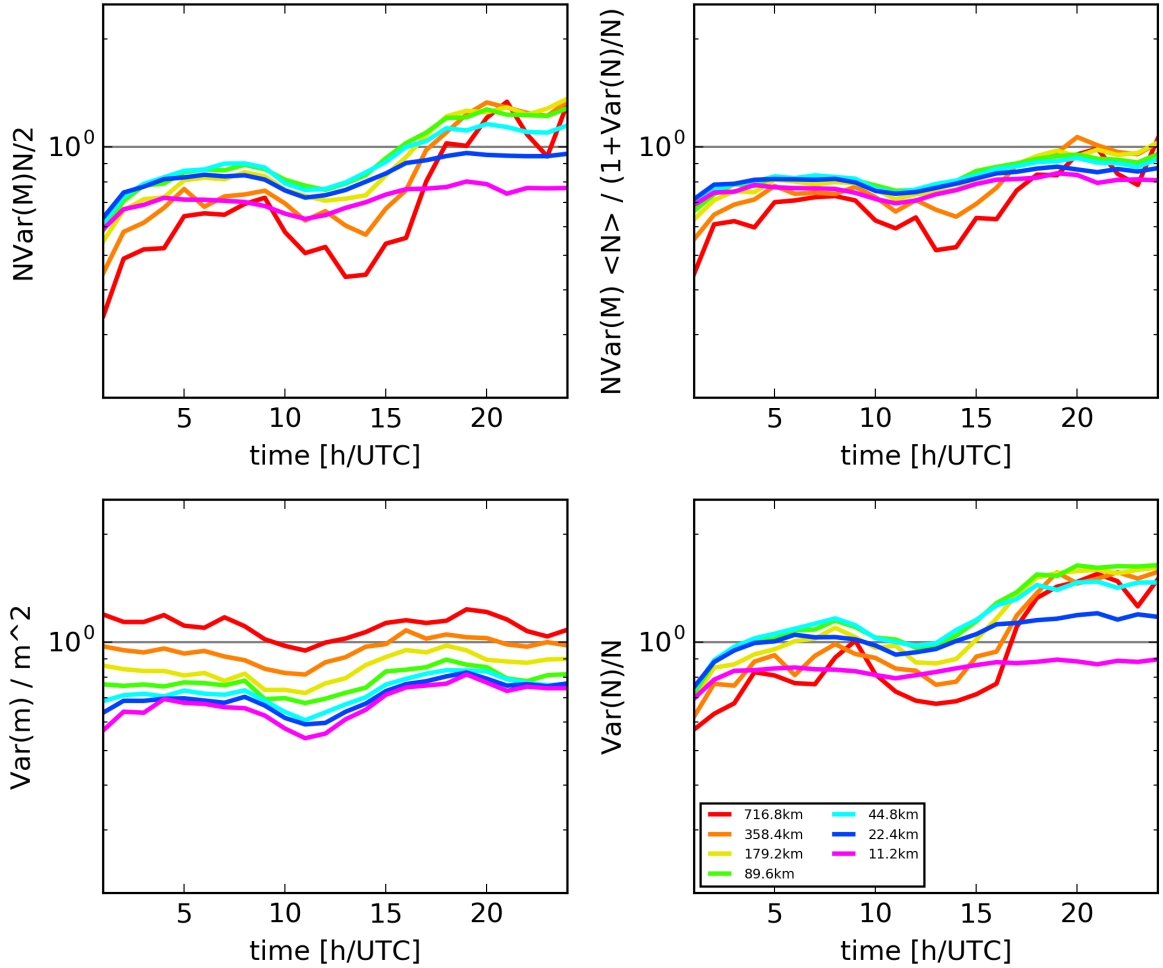


Figure 11: Time evolution of (top left) $0.5 \times \overline{\mu_2 \langle N \rangle}_n$ (see Eq. 16), (top right) $\frac{\tilde{\mu}_2 \langle N \rangle}{1+\alpha}_n$ (see Eq. 23), (bottom left) $\frac{1}{N_{\text{box}} n} \sum_{j=1}^{N_{\text{box}} n} \frac{\langle (\delta m)^2 \rangle_{j,n}}{\langle m \rangle_{j,n}^2}$ (see Eq. 20) and (bottom right) $\bar{\alpha}_n$ (see Eq. 18)

l00_201606100_201606200_201606300_201606400_20
 m, water=True, lev= 24, nens=20

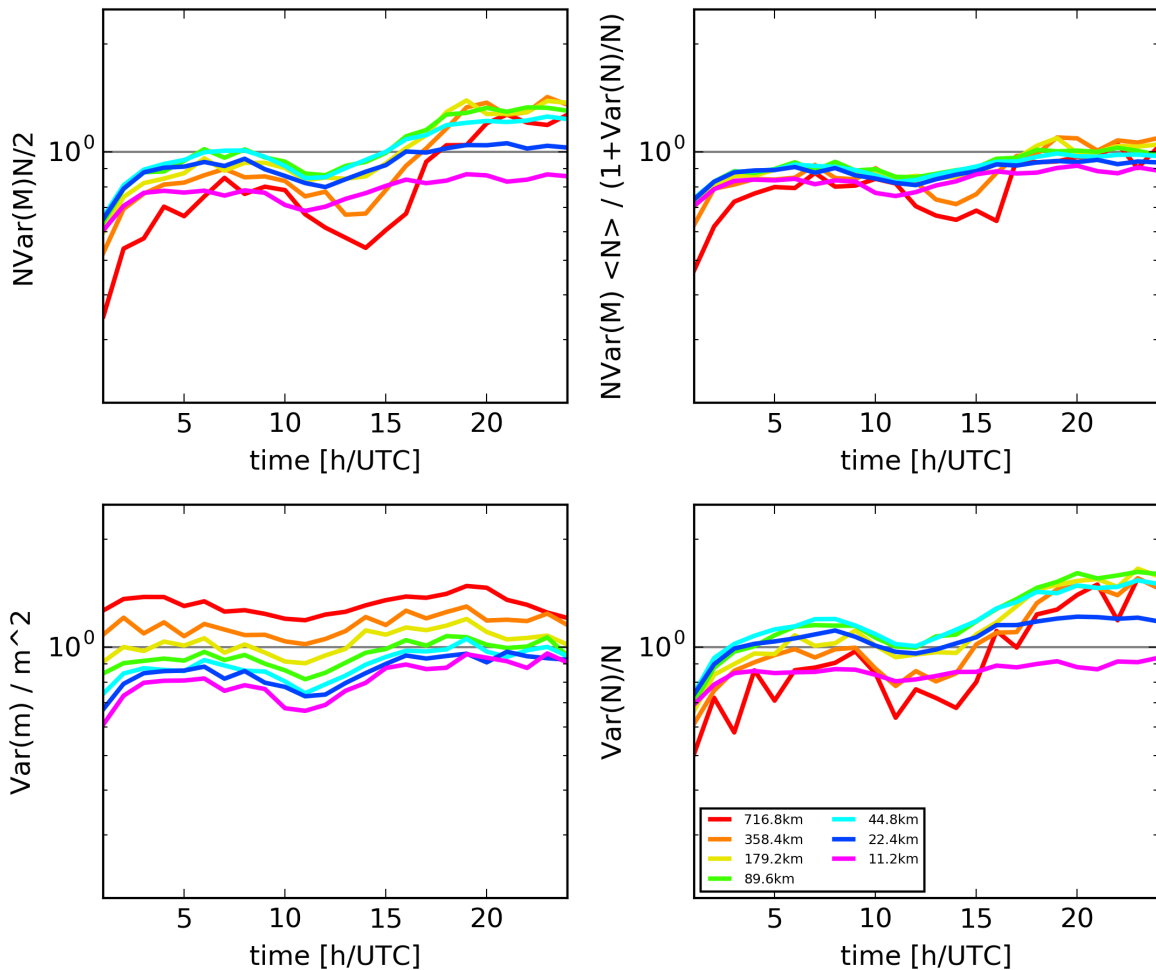


Figure 12: Same as above but at level 24 (about 5000m)

l00_201606100_201606200_201606300_201606400_20
 m, water=True, lev= 34, nens=20

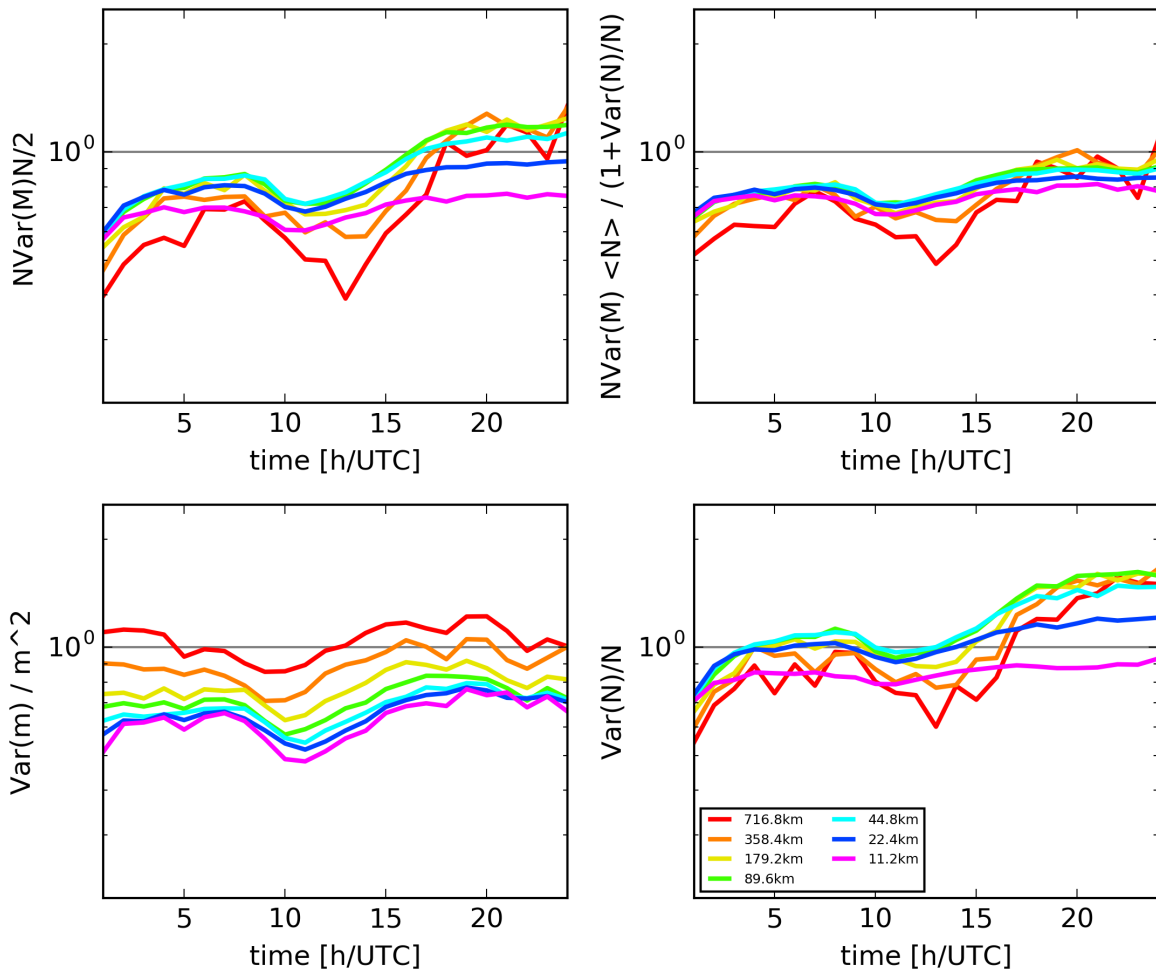


Figure 13: Same as above but at level 34 (about 2000m)